Hindawi Publishing Corporation
Journal of Nanomaterials
Volume 2011, Article ID 657516, 6 pages
doi:10.1155/2011/657516

Research Article

Synthesis and Characterization of Nanometer $Ce_{0.75}Zr_{0.25}O_2$ Powders by Solid-State Chemical Reaction Method

Yuying Zheng,[1] Zhengfa Hu,[2] Huimin Huang,[1] Wenjin Ji,[1] Ming Sun,[1] and Changshui Chen[3]

[1] *College of Light and Chemical Engineering, Guangdong University of Technology, Guangzhou, 510006, China*
[2] *College of Physics and Optoelectronics Engineering, Guangdong University of Technology, Guangzhou, 510006, China*
[3] *School of Information and Optoelectronic Science and Engineering, South China Normal University, Guangzhou, 510631, China*

Correspondence should be addressed to Yuying Zheng, zyyzhengyuyying@163.com and Zhengfa Hu, zhfhu@gdut.edu.cn

Received 8 May 2010; Revised 8 July 2010; Accepted 24 August 2010

Academic Editor: Bo Zou

The nanostructure $Ce_{0.75}Zr_{0.25}O_2$ powders have been successfully synthesized by using the mechanically activated solid-state chemical reaction method for the first time, with $Ce_2(CO)_3$, $ZrOCl_2 \cdot 8H_2O$, and $H_2C_2O_4 \cdot 2H_2O$ as raw materials. The structure and morphology of $Ce_{0.75}Zr_{0.25}O_2$ powders were characterized to be in the single cubic phase and spherical shape via X-ray powder diffraction, transmission electron microscopy, X-ray Photoelectron Spectrometer, and BET surface area testing technique. The average size of particles was measured to be less than 20 nm, and the specific surface area was 85.4 m_2/g. The TG-DTA investigation was used to reveal the possibly chemical reaction mechanism during the synthesis process. The activity of $Ce_{0.75}Zr_{0.25}O_2$ oxide solution in three-way catalysts was also valued in this work.

1. Introduction

The nanostructure, $Ce_{1-x}Zr_xO_2$ materials have drawn extraordinary research interests in recent years due not only to its good mechanical and electrical properties [1–4], but also to the potentials of applications in various fields, such as the catalysts [5–7], solid oxide electrolyte materials [8–10], and advanced ceramics [11–13], There have been many methods to prepare nano-$Ce_{1-x}Zr_xO_2$ solid solution, such as coprecipitation [14, 15], sol-gel [16, 17], high-temperature calcinations [18], high-energy mechanical milling, and hydrothermal method [19]. However, the procedure of the above approaches is so complicated that they are inevitably limited to apply to industrial and commercial situations.

Although substantial efforts have been exerted to the development of new synthetic methodologies for both efficiently making nano-$Ce_{1-x}Zr_xO_2$ and greatly lowering the synthesis costs, big difficulties still exist in the industrialization and productivity of each method. So far, the mechanically activated solid state chemical reaction method has gradually become a novel synthesis way that it exhibited high efficiency and lower cost of water and energy [20]. By comparing with other methods, the mechanically activated solid state chemical reaction method was considered to be a more simple industrial art without needing of plenty of solvents. In this work, the nanostructured $Ce_{0.75}Zr_{0.25}O_2$ was prepared by the mechanically activated solid state chemical reaction method for the first time. The characterization and properties of nano-$Ce_{0.75}Zr_{0.25}O_2$ were investigated and determined. Their catalysis efficiency was also checked at the aspect of potential applications.

2. Experimental

2.1. Preparation

2.1.1. Synthesis of Nano-$Ce_{1-x}Zr_xO_2$ Powders. The particles of nano-$Ce_{0.75}Zr_{0.25}O_2$ were prepared by mechanically activated solid-state chemical reaction method for the first time. At first, precursors were prepared by mixing of $ZrOCl_2 \cdot 8H_2O$, $Ce_2(CO_3)_3$ and $H_2C_2O_4 \cdot 2H_2O$ at the molar

ratio of $n(ZrOCl_2 \cdot 8H_2O)$: $n(Ce_2(CO_3)_3)$: $n(C_2H_2O_4 \cdot 2H_2O)$ = 0.25: 0.375: 0.375, then, the precursors were placed into the ball mill (model No. XQM-4L), operating at the initial angular speed 150 r/min for 2 hour. The amount of grinding media was kept a ratio of 10 : 1 to precursors. After one and a half hours grinding, the surfactant (5% total weight) was doped into the ball milling pot. At last the white resultant composition was calcined for 3 hours at the temperature of 600°C, and the yellow nanoparticles of $Ce_{0.75}Zr_{0.25}O_2$ were obtained.

2.1.2. Preparation of Catalysts. Catalyst A was mainly composed of the two noble metals totally taking a fraction 0.40% of weight in the three-way catalyst (TWC) [21, 22]. Pd and Rh took 0.25% and 0.15%, respectively. Here the preparation was briefly outlined Firstly, $Ce_{0.75}Zr_{0.25}O_2$ were blended with γ-Al_2O_3 under mechanical mixing, which only takes 30% of total weight. Secondly, the mixture of water solutions of $PdCl_2$ and $RhCl_3$ was prepared at the mass ratio of $m(Pd^{2+})$ and $m(Rh^{3+})$ = 5 : 3; then the mixture of water solutions of Pd- and Rh-contained salts was loaded into the mixture of $Ce_{0.75}Zr_{0.25}O_2$ and γ-Al_2O_3 for necessary reactions by incipient wetness method. Finally, the composite was calcined at 500°C for 2 hours and subsequently reduced at 500°C under atmosphere of H_2 for 2 hours.

Preparation of catalyst B. The preparation process was almost the same as catalyst A. The difference was that nano-$Ce_{0.75}Zr_{0.25}O_2$ powders were prepared by coprecipitation method, within which, $Ce(NO_3)_3 \cdot 8H_2O$ and $ZrOCl_2 \cdot 8H_2O$ were firstly dissolved inwater, respectively, to form water solutions both in 0.2 mol/L, and then they were mixed together. Subsequently, aqueous ammonia in 1 mol/L was poured into the solutions mixtures until the pH = 9.8 under continuously stirring. Finally, precipitate was washed and dried, then calcined at 600°C for 3 hours.

2.2. Characterization. TG-DTA analysis was performed based on SPA409PC analytic apparatus operated at the 30 mL/min airflow rate and the 5°C/min temperature rise rate. X-ray powder diffraction (XRD) measurements were made with a Rigaku D/Max-3B diffractometer employing Cu-Kα radiation. Transmission electron microscopy (TEM) (JEM-100CXII) was used to study the crystallization property and the size of the particles. Particle size distribution histograms were obtained on the basis of measurements from about 300 particles. X-ray photoelectron spectra (XPS) were recorded on an Scanning ESCA Microprobe (Quantum-2000, PHI) photoelectron spectrometer using Al-Kα radiation under a vacuum environment of 1×10^{-6} Pa. The binding energy of C_{1s} (284.6 eV) was used for the calibration of all binding energies. The specific surface area (S_{BET}) of the products was checked by measuring the adsorptive capacity of N_2 at −196°C by using full-automatic adsorption instrument ASAP2010M.

2.3. Catalysis. As for the activity of catalysts, it was evaluated by monitoring the contents of five components such as NO, CH, CO, O_2, and CO_2 in automobile exhaust gas by using gas chromatograph (GC 9790) and the automobile exhaust analytic system(FGA-4100), with the reference exhaust composed of $\varphi(NO)$ = 0.1%, $\varphi\{CH[V(C_3H_8) : V(C_3H_6) = 1 : 1]\}$ = 0.1%, $\varphi(CO)$ = 1.5%, and $\varphi(O_2)$ = 1.37% in volume fraction. The instruments were run with He as buffer gas at S.V. = 40000 h^{-1} and air/fuel (A/F) ratio of 14.6. The temperature rise rate was set at 10°C per minute. The rate of conversion could be calculated as following:

$$X = \frac{\sigma_0 - \sigma_1}{\sigma_0} \times 100\%, \quad (1)$$

where X denotes the rate of conversion, σ_0 and σ_1 stand by the starting volume fraction and final volume fraction of gases, respectively.

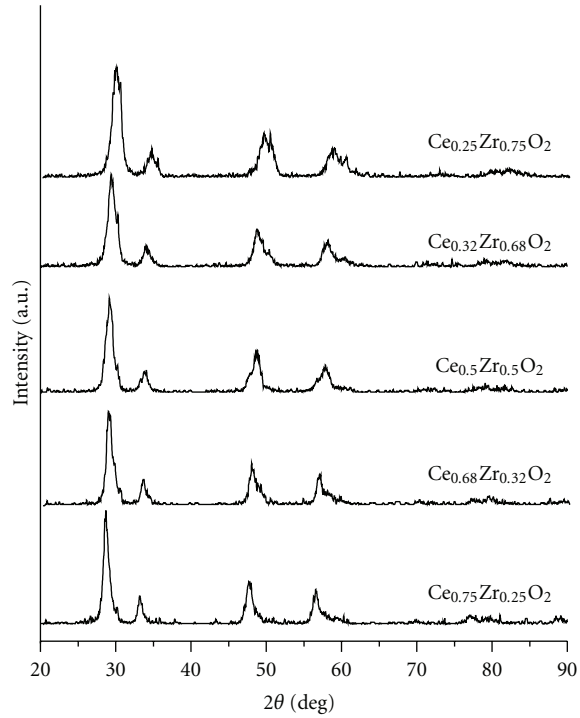

Figure 1: XRD spectra of $Ce_xZr_{1-x}O_2$ solid solutions.

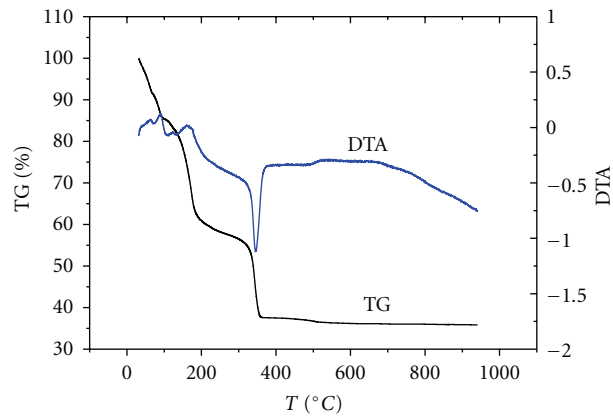

Figure 2: TG-DTA curves of the precursors.

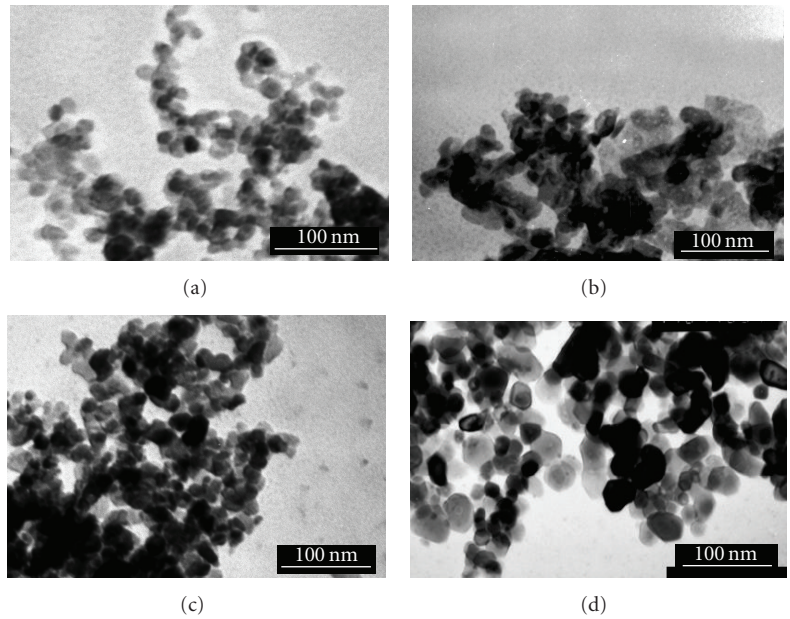

Figure 3: TEM images of $Ce_{0.75}Zr_{0.25}O_2$ produced under surfactants (a) Tween-60, (b) neopelex, (c) PEG-400, and (d) CTAB.

Table 1: Different molar ratios of raw materials correspond to different products and particle size.

Sample No.	Molar ratio of raw materials $ZrOCl\cdot 8H_2O$:$Ce_2(CO_3)_3$:$C_2H_2O_4\cdot 2H_2O$	Product	Crystal volume (nm^3)
1	0.25 : 0.375 : 0.375	$Ce_{0.75}Zr_{0.25}O_2$	0.15141
2	0.32 : 0.34 : 0.48	$Ce_{0.68}Zr_{0.32}O_2$	0.14595
3	0.5 : 0.25 : 0.75	$Ce_{0.5}Zr_{0.5}O_2$	0.14310
4	0.68 : 0.16 : 1.02	$Ce_{0.32}Zr_{0.68}O_2$	0.14198
5	0.75 : 0.125 : 1.125	$Ce_{0.25}Zr_{0.75}O_2$	0.14012

3. Results and Discussion

3.1. Determination of Solid Solution Manner. Figure 1 and Table 1 displayed that XRD patterns of the final products prepared from the different ratio of raw materials, and the corresponding crystal volumes, respectively. As can be seen, the crystal volume decreases gradually with the increment of the concentration of Zr^{4+} ions. In general, there are two ways that Zr^{4+}ions could be doped into the crystal lattice of CeO_2, one is that Zr^{4+} is filled into the crystal lattice in the form of gap ions, the existence of Zr^{4+} ion thus causes a vacancy of Ce^{4+}, leading to enlargement of the volume of $Ce_{1-x}Zr_xO_2$ crystal cell. The other is that Zr^{4+} fully substituted for Ce^{4+} leading to the compactness of the crystal lattice as the ionic radius of Zr^{4+}(0.079 nm) is less than that of Ce^{4+} (0.092 nm). The experimental results obviously showed that the lattice constant (d_{XRD}) declined with the increasing amount of Zr^{4+}, in accordance with the second doping manner of Zr ions, namely, Ce^{4+} ions in CeO_2 were partially replaced by Zr^{4+} in the $Ce_{1-x}Zr_xO_2$ solid solution, resulting in the reduction of the crystal volume.

XRD patterns of $Ce_{0.75}Zr_{0.25}O_2$ solid solution in Figure 1 indicated that $Ce_{0.75}Zr_{0.25}O_2$ solid solution has a crystal structure in a cubic phase. From the analysis of XRD pattern, we could calculate the d_{XRD} and the degree of crystallization (X_c). The X_c was calculated according to

$$X_c = \frac{I_c}{I_c + I_a} \times 100\%, \tag{2}$$

where I_c denotes the area of crystallinity phase, and I_a stands for the area of amorphous phase. As a result, the d_{XRD} and the degree of crystallization (X_c) were obtained to be 14.46 nm and 95.3%, respectively. No peak of impurity was found in the XRD patterns referenced by the standard card 28-271 in Powder Diffraction File (PDF).

3.2. TG-DTA Analysis. The TG-DTA data were plotted in Figure 2. The TG curve displayed three main stages through the whole process. Loss of free water from precursors surface firstly took place at about 116°C. A further loss of weight followed, as seen from the exothermic peak on the DTA curve at 170°C. Continuous loss of water from oxalate and heat decomposition of excessive oxalic acid resulted in the reduction of weight. The loss of weight was up to about 22% after this step. Then the heat decomposition of oxalate began

Table 2: Referenced binding energy of Zr 3d, Ce 3d, and O 1s in oxides [23].

Element	Core level	Oxide	Binding energy/eV
Zr	$3d_{5/2}$	ZrO_2	183.1
Zr	$3d_{3/2}$	ZrO_2	185.5
Zr	$3d_{3/2}$	$ZrO_2/(CeO_x+Y_2O_3+ZrO_2)$	182.6
Ce	$3d_{5/2}$	$Ce_2O_3/(CeO_x+Y_2O_3+ZrO_2)$	885.6
Ce	$3d_{3/2}$	$Ce_2O_3/(CeO_x+Y_2O_3+ZrO_2)$	903.7
Ce	$3d_{5/2}$	$CeO_2/(CeO_x+Y_2O_3+ZrO_2)$	882.4
Ce	$3d_{3/2}$	$CeO_2/(CeO_x+Y_2O_3+ZrO_2)$	900.9
Ce	$3d_{5/2}$	CeO_2	881.8
Ce	$3d_{3/2}$	CeO_2	916.7
Ce	$3d_{5/2}$	Ce_2O_3	880.7
O	1s	$CeO_2/(CeO_x+Y_2O_3+ZrO_2)$	530.0
O	1s	$Ce_2O_3/(CeO_x+Y_2O_3+ZrO_2)$	532.0

Table 3: Light-off temperature of catalysts A and B.

Catalyst	T_{50} (CH)/°C	T_{50} (CO)/°C	T_{50} (NO)/°C
A	295.7	239.1	230.6
B	293.2	239.2	231.8

and lasted from 240°C to 600°C, resulting in the reduction of the precursors weight by 26.5%, which was basically consistent with the theoretical the loss of weight of 27.7%. According to the TG-DTA analysis, the following chemical reactions occurred within the process of heat decomposition:

$$ZrOC_2O_4 \cdot 2H_2O + O_2 \longrightarrow ZrO_2 + 2CO_2 \uparrow + 2H_2O, \quad (3)$$

$$2Ce_2(CO_3)_3 + O_2 \longrightarrow 4CeO_2 + 6CO_2, \quad (4)$$

$$(1 - x)CeO_2 + xZrO_2 \longrightarrow Ce_{1-x}Zr_xO_2, \quad (5)$$

Equations (3) and (4) indicated the heat decomposition reactions, whilst (5) showed the stoichiometric reaction without the loss of weight. As shown in Figure 1, $Ce_2(CO_3)$ was not involved in the reaction with $H_2C_2O_4 \cdot 2H_2O$, only $ZrOCl_2 \cdot 8H_2O$ reacted with $H_2C_2O_4 \cdot 2H_2O$ during the process of ball milling.

3.3. Influence of Surfactant. In order to avoid the aggregation, the influence of surface active agents onto the product was also investigated. TEM images of the nanosized samples, prepared under the introduction of different surface active agents to the precursors, were shown in Figure 3, indicating the effect of different surfactants onto the crystallization property and the size of the particles. The cationic surfactant of hexadecyl trimethyl ammonium bromide (CTAB) showed no distinct effect. The anionic surfactant of neopelex made the particles size rise up to 37.4 nm. On the contrary, the neutral surfactants PEG-400 and Tween-60 enabled the particles to maintain relatively small sizes of less than 25 nm and more homogeneous distributions. With tween-60 as surfactant, the property of the particles was superior to those prepared under other surface active agents. The experimental results demonstrated that the particles were in more uniformly spherical shape with homogeneous dispersion. The average size of particles was obtained to be less than 20 nm, and the S_{BET} was 85.4 m^2/g, obviously larger than the S_{BET} of 60.2 m^2/g, 76.9 m^2/g, and 69.7 m^2/g, corresponding to surfactants (b), (c), and (d) in Figure 3.

The experimental results also indicated that the neutral surfactant could effectively prevent the aggregation of particles such that the particle size could be well controlled. The nonionic surfactant was hardly affected by the inorganic ions during the grind and could facilitate the formation of hydrogen bond, thus a protectively hydrophilic film was easily formed on the surface of the powder. The hydrophilic film enabled the powders to have spatially steric hindrance and electrostatic effects, preventing product particles from aggregation into large size. However, the cationic surfactant could easily react with the $H_2C_2O_4 \cdot 2H_2O$ due to the alkalinity, so that no obvious effect was brought onto the particles. The anionic surfactant could cause the rising of the particles sizes.

3.4. XPS Analysis. The XPS spectra of Zr 3d, Ce 3d, and O 1s in $Ce_{0.75}Zr_{0.25}O_2$ oxides were displayed in Figure 4. The binding energies of Zr 3d, Ce 3d, and O 1s in oxides were listed in Table 2 for reference and comparison [23]. Based on the fitting of XPS spectra with a Gaussian shape, we obtained the binding energies (E_b) of Ce $3d_{5/2}$ and $Ce3d_{3/2}$ to be 882.42 eV and 900.85 eV, respectively, comparatively close to the reference $E_b(Ce3d_{5/2})$ = 884.98 eV and $E_b(Ce3d_{3/2})$ = 903.68 eV measured in solid solution of oxides $CeO_2/(CeO_x+Y_2O_3+ZrO_2)$ and $Ce_2O_3/(CeO_x+Y_2O_3+ZrO_2)$, respectively. So it was reasonable to believe that both Ce^{3+} and Ce^{4+} exist in the products. E_b (Zr 3d) was measured to be 182.6 eV, equal to the binding energy of Zr 3d in $ZrO_2/(CeO_x+Y_2O_3+ZrO_2)$. As for the E_b (O 1s), two binding energies, 529.98 eV and 532.03 eV, were obtained, corresponding to 530.0 and

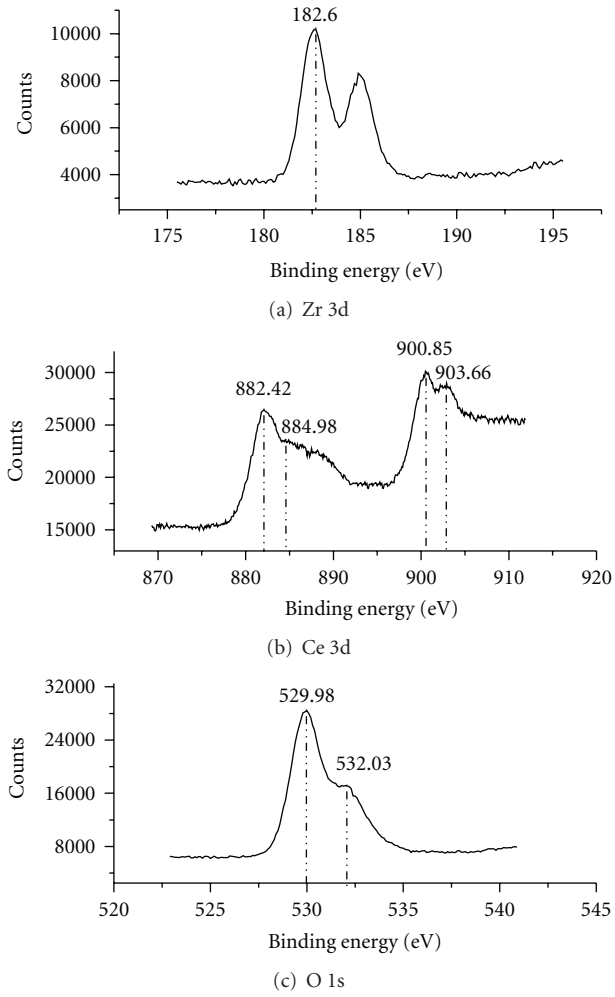

Figure 4: XPS spectra of Zr 3d, Ce 3d and O 1s in $Ce_{0.75}Zr_{0.25}O_2$.

532.0 eV in solid solution of $CeO_2/(CeO_x+Y_2O_3+ZrO_2)$ and $Ce_2O_3/(CeO_x+Y_2O_3+ZrO_2)$, respectively. These facts proved that the products prepared by mechanically activated solid state chemical reaction to be in the state of solid solution of oxides, which was favored by the XRD results.

3.5. Evaluation of Catalyst. Catalyst A and B were used to decontaminate the automotive exhaust. The catalysis efficiency was determined by monitoring the contents of greenhouse gas, such as NO, CH, and CO, through the conversion rate. The conversion rates in percentage of NO, CH and CO have been calculated according to (1) and shown in Figure 5. The light-off temperatures (T_{50}) of the above gases were listed in Table 3. As seen from Figure 5 and Table 3, no obvious difference could be found between the two catalysts, except for the fluctuation of $1 \sim 2^{\circ}C$ at the light-off temperature. Although the two catalysts, prepared by different methods, they almost had the same catalysis function. The mechanically activated solid state chemical reaction method still possessed obvious advantages of easily manufacturing, energy saving, and less solvent, indicating its promisingly commercial and industrial potentials.

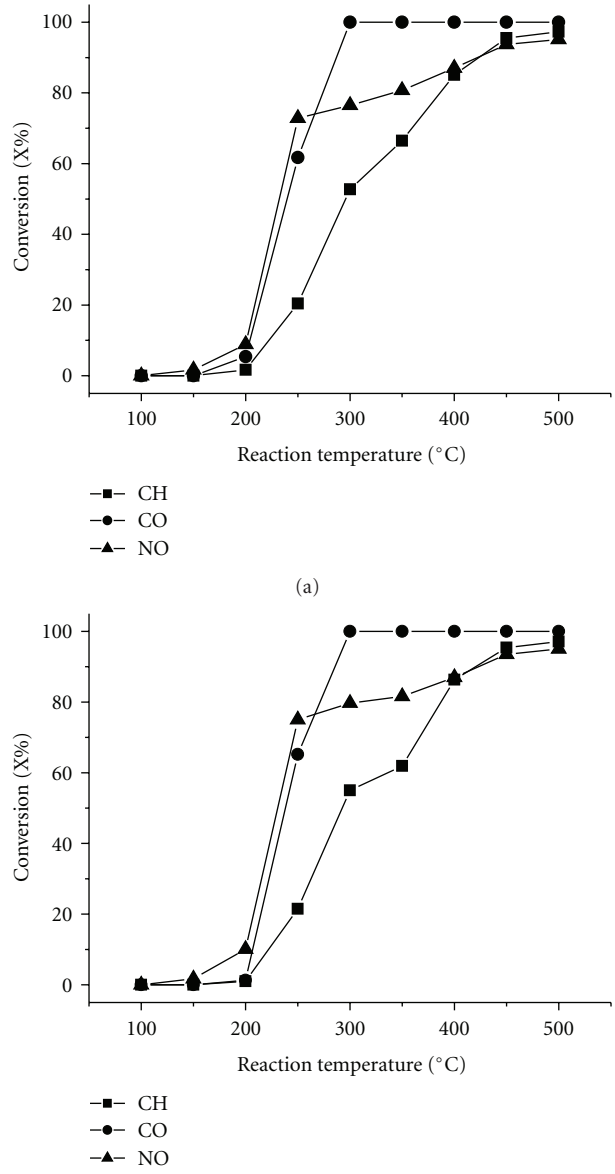

Figure 5: The catalysis activity of catalyst (a) and (b).

4. Conclusion

In summary, Nano-$Ce_{0.75}Zr_{0.25}O_2$ powders were prepared by using the solid-solid chemical reaction method under the action of mechanical power. The products were determined to be in the single-cubic-phase. The particles were found to be in more spherical shape with the average size less than 20 nm, the better specific surface area of 85.4 m^2/g, and more uniform dispersion.

The effects of surfactants employed in the synthesis process of the products have also been investigated. The facts proved that Tween-60 and PEG-400 had better effects on the control of particle sizes.

The mechanically activated solid state chemical reaction method possessed obvious advantages in manufacturing, energy-saving, and less solvent.

Acknowledgments

This work was supported financially by Government of Guangdong Province for 211 Subject Construction. The authors are also grateful to the financial support from National Natural Science Foundation of China (NSFC) under Grant no. 60977029, 10774031, and 60878063, and from High Technology Research Program 2007AA021806. Y. Zhang and Z. Hu equally contributed to this work.

References

[1] W. J. Stark, M. Maciejewski, L. Mädler, S. E. Pratsinis, and A. Baiker, "Flame-made nanocrystalline ceria/zirconia: structural properties and dynamic oxygen exchange capacity," *Journal of Catalysis*, vol. 220, no. 1, pp. 35–43, 2003.

[2] S. K. Tadokoro and E. N. S. Muccillo, "Physical characteristics and sintering behavior of ultrafine zirconia-ceria powders," *Journal of the European Ceramic Society*, vol. 22, no. 9-10, pp. 1723–1728, 2002.

[3] S. Bernal, G. Blanco, J. J. Calvino et al., "Some recent results on the correlation of nano-structural and redox properties in ceria-zirconia mixed oxides," *Journal of Alloys and Compounds*, vol. 451, no. 1-2, pp. 521–525, 2008.

[4] E. N. S. Muccillo and D. M. Ávila, "Impedance spectroscopy of tetragonal zirconia polycrystals doped with ceria," *Materials Letters*, vol. 56, no. 4, pp. 454–459, 2002.

[5] A. Martorana, G. Deganello, A. Longo et al., "Structural evolution of Pt/ceria-zirconia TWC catalysts during the oxidation of carbon monoxide," *Journal of Solid State Chemistry*, vol. 177, no. 4-5, pp. 1268–1275, 2004.

[6] M. LI, Z. LIU, Y. HU, M. WANG, and H. LI, "Effect of doping elements on catalytic performance of CeO_2-ZrO_2 solid solutions," *Journal of Rare Earths*, vol. 26, no. 3, pp. 357–361, 2008.

[7] J. A. Wang, T. López, X. Bokhimi, and O. Novaro, "Phase composition, reducibility and catalytic activity of Rh/zirconia and Rh/zirconia-ceria catalysts," *Journal of Molecular Catalysis A*, vol. 239, no. 1-2, pp. 249–256, 2005.

[8] N. M. Sammes and C. Zhihong, "Ionic conductivity of ceria/yttria stabilized zirconia electrolyte materials," *Solid State Ionics*, vol. 100, no. 1-2, pp. 39–44, 1997.

[9] C. H. Lee and G. M. Choi, "Electrical conductivity of CeO_2-doped YSZ," *Solid State Ionics*, vol. 135, no. 1–4, pp. 653–661, 2000.

[10] Q. X. Fu, W. Zhang, R. R. Peng, D. K. Peng, G. Y. Meng, and B. Zhu, "Doped ceria-chloride composite electrolyte for intermediate temperature ceramic membrane fuel cells," *Materials Letters*, vol. 53, no. 3, pp. 186–192, 2002.

[11] E. N. S. Muccillo and D. M. Ávila, "Synthesis and characterization of submicron zirconia-12 mol% ceria ceramics," *Ceramics International*, vol. 25, no. 4, pp. 345–351, 1999.

[12] W. Pyda, K. Haberko, and Z. Zurek, "Zirconia stabilized with a mixture of the rare earth oxides," *Journal of the European Ceramic Society*, vol. 10, no. 6, pp. 453–459, 1992.

[13] Y. L. Zhang, X. J. Jin, and T. Y. Hsu, "Thermodynamic calculation of Ms in ZrO_2-CeO_2-Y_2O_3 system," *Journal of the European Ceramic Society*, vol. 23, no. 5, pp. 685–690, 2003.

[14] S. Rossignol, Y. Madier, and D. Duprez, "Preparation of zirconia-ceria materials by soft chemistry," *Catalysis Today*, vol. 50, no. 2, pp. 261–270, 1999.

[15] C. LI, X. GU, Y. WANG et al., "Synthesis and characterization of mesostructured ceria-zirconia solid solution," *Journal of Rare Earths*, vol. 27, no. 2, pp. 211–215, 2009.

[16] K. S. Kumar and T. Mathews, "Sol-gel synthesis and microwave assisted sintering of zirconia-ceria solid solution," *Journal of Alloys and Compounds*, vol. 391, no. 1-2, pp. 177–180, 2005.

[17] X. Wu, J. Fan, R. Ran, and D. Weng, "Effect of preparation methods on the structure and redox behavior of platinum-ceria-zirconia catalysts," *Chemical Engineering Journal*, vol. 109, no. 1, pp. 133–139, 2005.

[18] C. E. Hori, H. Permana, K. Y. S. Ng et al., "Thermal stability of oxygen storage properties in a mixed CeO2-ZrO2 system," *Applied Catalysis B: Environmental*, vol. 16, no. 2, pp. 105–117, 1998.

[19] S. Enzo, R. Frattini, F. Delogu, A. Primavera, and A. Trovarelli, "Neutron diffraction studies of ceria-zirconia catalysts prepared by high-energy mechanical milling," *Nanostructured Materials*, vol. 12, no. 5, pp. 673–676, 1999.

[20] Q. Q. Tan, Z. L. Tang, and Z. T. Zhang, "Preparation and microstructure of nanometer tetragonal polycrystal zirconia powder at low temperature condition," *Journal of Materials Engineering*, vol. 11, p. 57, 2004.

[21] S. S. Deshmukh, M. Zhang, V. I. Kovalchuk, and J. L. D'Itri, "Effect of SO_2 on CO and C_3H_6 oxidation over CeO_2 and $Ce_{0.75}Zr_{0.25}O_2$," *Applied Catalysis B*, vol. 45, no. 2, pp. 135–145, 2003.

[22] H. S. Gandhi, G. W. Graham, and R. W. McCabe, "Automotive exhaust catalysis," *Journal of Catalysis*, vol. 216, no. 1-2, pp. 433–442, 2003.

[23] NIST X-ray Photoelectron Spectroscopy Database, http://srdata.nist.gov/xps/.